Fractional robust control of a nonlinear plant

Control of a nonlinear testing bench using the singular perturbation technique and the CRONE approach

Valérie Pommier-Budinger * — Patrick Lanusse — Jocelyn Sabatier**— Alain Oustaloup****

** ENSICA*
1, Place Blouin, 31056 Toulouse - France
e-mail: valerie.pommier@ensica.fr

*** LAPS UMR 5131 CNRS/Université Bordeaux I/ENSEIRB*
351, Cours de la Libération, 33405 Talence - France

ABSTRACT. The control of a hydraulic testing bench is presented by using both singular perturbations technique and Crone control (fractional robust control). The testing bench is constituted of a hydraulic actuator which deforms, with a required velocity, the uncertain mechanical structures to be tested. Thanks to the singular perturbations techniques, the plant can be linearized despite the uncertainty by using a simplified input-output linearization under diffeomorphism and feedback. The Crone control is used to reject remaining nonlinearities considered as perturbations and to control the actuator velocity while taking into account the parametric variations of the mechanical structures.

MOTS-CLES: *perturbations singulières, commande d'ordre non entier; système non linéaire; linéarisation par retour; banc d'essais hydraulique.*

KEYWORDS: *singular perturbation; fractional order control; nonlinear system; feedback linearization; hydraulic testing bench.*

1. Introduction

This paper presents the velocity control of a hydraulic actuator that is part of a testing bench for mechanical structures. The difficulty of this problem of control comes from the nonlinearity of the actuator and from the uncertainty on the model of the mechanical structure to be tested. The proposed control-system design is the CRONE control which is a frequency-domain based methodology to design robust linear controller using fractional differentiation. Considering the robustness/performance trade-off, the plant perturbations are taken into account by using fully-structured frequency uncertainty domains to obtain the least-conservative controllers (Landau *et al*, 1995).

The strategy to control non linear systems with a linear control-system design comprises two steps (linearizing the system and computing the control law) and then leads to a control scheme with two feedback loops (Fig. 1)

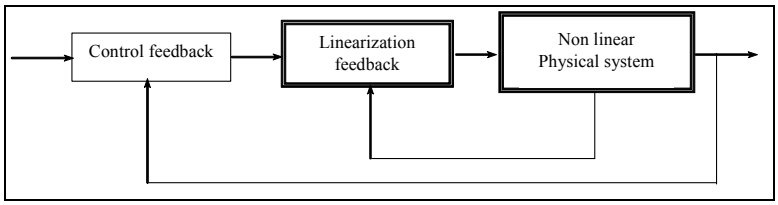

Figure 1. *Strategy of control*

The linearization feedback which transforms the nonlinear model of the actuator into a linear model can be achieved thanks to an input-output linearization technique (Isidori, 1989) (Krstic *et al*, 1995) (Fossard *et al*, 1997) (Lanusse *et al*, 2000). But when the plant under consideration is perturbed, the input-output linearization - that can be achieved only for one state - leaves the plant nonlinear for the other states. Previous works using this strategy have already been achieved (Banavar *et al*, 1998) (Lanusse *et al*, 2000) (Pommier *et al*, 2001).

In this article, another technique of linearization is adopted. The linearization is achieved thanks to the singular perturbation technique. This technique presents two advantages.

First, by considering the electrohydraulic system as a two time-scales singular perturbed dynamic system, it is possible to compute a linearization feedback that is independent of the uncertain parameters of the mechanical structure to be tested. The obtained linear plant is thus available whatever the mechanical structure.

Secondly, the linearization feedback obtained with the perturbation technique is simpler to implement than the one obtained without considering a two time-scales dynamic system. As it is true that the perturbation technique is based on some assumptions, the linearization may not be totally achieved. The remaining plant nonlinearities are considered as perturbations that will be taken into account in the CRONE robust control loop at the same time as the uncertainty on the mechanical structure.

The article is organized as follows. Section 2 reminds of the singularly perturbed system and explains how this technique can be used to simplify the input-output linearization. Section 3 presents the Crone control-system design method. Section 4 first gives a description and a model of the electrohydraulic test bench. Then the singular perturbation technique is applied to the test bench and the input-output linearization is described. In section 5, the control of the testing bench is developed and realistic simulation results are given.

2. Singular perturbation technique

2.1. *Definition (Fossard* et al*, 1997)*

A singularly perturbed dynamic system is a system where state equations can be written in the standard form:

$$\begin{aligned} \dot{\mathbf{X}}_s &= \mathbf{f}_s(\mathbf{X}_s, \mathbf{X}_f, \mathbf{u}, \varepsilon) \\ \varepsilon\dot{\mathbf{X}}_f &= \mathbf{f}_f(\mathbf{X}_s, X_f, \mathbf{u}, \varepsilon) \end{aligned}, \qquad [1]$$

where $\mathbf{X}_s \in \mathrm{R}^q, \mathbf{X}_f \in \mathrm{R}^p, \mathbf{f}_s, \mathbf{f}_f$ are regular vectorial functions in $\mathbf{X}_s, \mathbf{X}_f, \mathbf{u}, \varepsilon$ and where ε is a small positive parameter (suffix s is for slow and f for fast).

If ε is small enough, the system has two time-scales. The variation of velocity is different between $\boldsymbol{X}_s$ and $\boldsymbol{X}_f$. Rewriting the equations with the time-scale $\tau = \frac{t}{\varepsilon}$, system [1] becomes:

$$\begin{aligned} \frac{d\mathbf{X}_s}{d\tau} &= \varepsilon\mathbf{f}_s(\mathbf{X}_s, \mathbf{X}_f, \mathbf{u}, \varepsilon) \\ \frac{d\mathbf{X}_f}{d\tau} &= \mathbf{f}_f(\mathbf{X}_1, \mathbf{X}_2, \mathbf{u}, \varepsilon) \end{aligned}. \qquad [2]$$

When $\varepsilon \to 0$, the velocity of $\boldsymbol{X}_s$ tends to 0 while the velocity of $\boldsymbol{X}_f$ remains limited.

2.2. *Forced singular perturbations*

Writing a realistic physical system in a standard singularly perturbed form and separating the system into slow and fast variables can be complex from a mathematical point of view. In several practical cases, it is not possible to define a small parameter ε even though one knows through experience or through simulation that the system has indeed several dynamics, slow and fast ones. In such cases, the parameter ε is formally introduced, multiplying the derivatives of fast state variables in order to be treated afterwards as a real perturbation parameter. This technique is called "forced singular perturbations" (Fossard *et al*, 1997).

To help with the variables classifications, one can use the following definition of the "velocity" v_{x_i} of a variable x_i:

$$v_{x_i} = \max \left| \frac{f_i(X,u))}{\Delta x_i} \right| . \qquad [3]$$

2.3. *Application to the linearization by diffeomorphism and input-output feedback*

Taking into account two (or even more) time-scales can help with the analysis, simulation and control of a nonlinear system. Indeed by considering that some state variables are slow whereas other variables are fast, a global system can be separated into two subsystems (Fig.2). Thanks to this dynamic separation, slow variables are assumed to be constant for the fast subsystem and fast variables can be assumed as inputs for the slow subsystem. If the fast subsystem is nonlinear, it is then possible to compute an input-output feedback while considering only the fast state-variables and thus the feedback is simpler and more feasible.

Of course, as the dynamic separation can not be totally obtained, the linearization is only achieved approximately. The remaining nonlinearities can then be considered as perturbations that must be rejected by using a linear feedback.

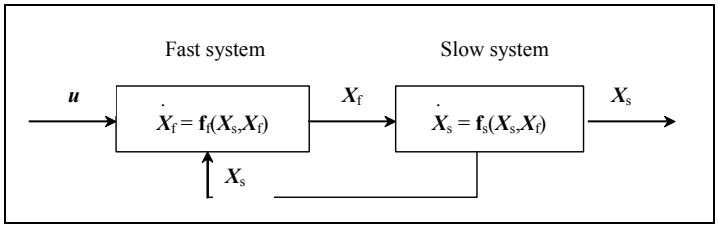

Figure 2. *Separation of a global system into slow and fast subsystems*

3. CRONE control-system design method

3.1. *Principles*

CRONE (the French acronym of "Commande Robuste d'Ordre Non Entier") control-system design (Oustaloup *et al*, 1995) (Oustaloup *et al*, 1999, 1) is a frequency-domain based methodology, using fractional differentiation (Miller *et al*, 1993) (Samko *et al*, 1993) (Oustaloup *et al*, 1999, 2). It permits the robust control of perturbed plants using the common unity feedback configuration. It consists on determining the nominal and optimal open-loop transfer function that guaranties the required specifications. While taking into account the plant right half-plane zeros and poles, the controller is then obtained from the ratio of the open-loop frequency response to the nominal plant frequency response. Three generations of Crone control-system design have been developed, successively extending the application fields. Crone control design has already been applied to unstable or non-minimum-phase plants, plants with bending modes (Landau *et al*, 1995) (Oustaloup *et al*, 1995), and digital control problems (Oustaloup *et al*, 1999, 1). In this paper, only the principle of the third generation is given. The interests of Crone control-system design are multiple. The use of complex fractional differentiation permits to define the open-loop transfer function with few high-level parameters. The optimization problem that leads to the optimal transfer function to meet the specifications is thus easier to solve. Moreover, Crone control design takes into account the genuine plant perturbation without over-estimation and then better performance can be obtained.

3.2. *Third generation Crone control-system design*

The third generation Crone method is based on a particular open-loop Nichols locus called a *generalized template* and defined by a any-direction straight line segment around open-loop gain crossover frequency ω_{cg} (Fig.3). This generalized template is based on the real part (with respect to imaginary unit i) of complex fractional integration (Oustaloup, 1995):

$$\beta(s)=\left[\cosh\left(b\frac{\pi}{2}\right)\right]^{-1}\Re_{/i}\left[\left(\frac{\omega_{cg}}{s}\right)^{n}\right], \qquad [4]$$

with $n=a+ib\in C_i$ and $s=\sigma+j\omega\in C_j$. In the Nichols chart at frequency ω_{cg}, the real order a determines the phase placement of the template, and then the imaginary order b determines its angle to the vertical (Oustaloup *et al*, 2000).

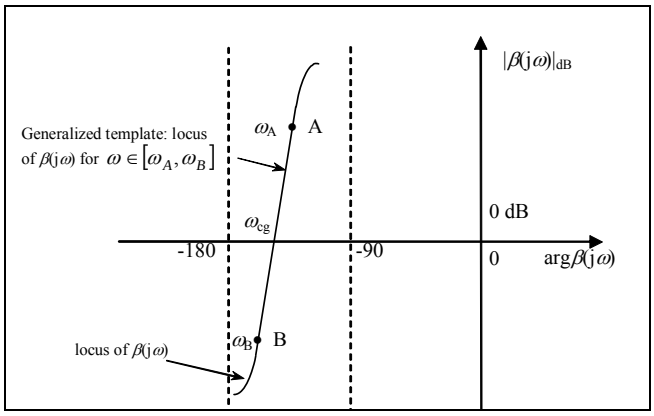

Figure 3. *Representation in the Nichols chart of the generalized template by an any-direction straight line segment*

In the version of third generation Crone control-system design used in this article, the open-loop transfer function defined for the nominal state of the plant, $\beta_o(s)$, takes into account the control specifications at low and high frequencies and a set of band-limited generalized templates around resonant frequency ω_r. Thus $\beta_o(s)$ is defined by:

$$\beta_0(s) = K\left(\frac{\omega_{-N^-}}{s}+1\right)^{n_l} \frac{1}{(1+s/\omega_{N^++1})^{n_h}} \prod_{-N^-}^{N^+}\left(\frac{1+s/\omega_{k+1}}{1+s/\omega_k}\right)^{a_k}\left(\Re_{/i}\left[\left(C_k\frac{1+s/\omega_{k+1}}{1+s/\omega_k}\right)^{ib_k}\right]\right)^{-\mathrm{sign}(b_k)} \quad [5]$$

where

$$C_0 = \left[\left(1+\omega_r^2/\omega_0^2\right)/\left(1+\omega_r^2/\omega_1^2\right)\right]^{1/2} \quad [6]$$

and

$$C_k = \left[\omega_{k+1}/\omega_k\right]^{1/2} \text{ for } k \neq 0 \cdot \quad [7]$$

K ensures a 0 dB gain of $\beta_0(\omega_{cg})$, the order n_l fixes the steady state behavior of the closed-loop system at low frequencies, and the value of n_h has to be chosen as equal to or greater than the high-frequency order of the plant.

Crone control design guaranties the robustness of both stability margins and performance, and particularly the robustness of the maximum M of the complementary sensitivity function magnitude. Let M_r be the required resonant magnitude peak of the complementary sensitivity function for the nominal

parametric state of the plant. An indefinite number of open-loop Nichols locus can tangent the Nichols magnitude contour of graduation M_r. Also, for uncertain plants, parametric variations lead to variations of M. Thus, an open-loop Nichols locus is defined as optimal if the generalized template around ω_r tangents the M_r Nichols magnitude contour for the nominal state and if it minimizes the variations of M for the other parametric states. By minimizing the cost-function $J = \left(M_{\max} - M_r\right)^2$ where $M_{\max}$ is the maximal value of resonant peaks M, the optimal open-loop Nichols locus positions the uncertainty domains correctly, so that they overlap the low stability margin areas as little as possible. The minimization of J is carried out under a set of shaping constraints on the four usual sensitivity functions. Once the optimal open-loop is obtained, the controller $C_f(s)$ deduced from the ratio of $\beta_o(s)$ to the nominal plant function transfer is a fractional transfer function with fractional order. The design of the achievable controller consists in replacing $C_f(s)$ by a rational controller $C_r(s)$ which has the same frequency response.

4. Electrohydraulic testing bench

4.1. *Description*

The testing bench is constituted of a electrohydraulic actuator connected to a mechanical structure (see Fig4). The electrohydraulic actuator must deform this structure with a velocity given in Fig.5. The actuator is a double-acting 200 mm stroke cylinder. A servo-valve fed with a hydraulic pump supplies a constant pressure. The mechanical structure is modeled by a mass-damper-spring set. The values of the structure's parameters vary during the test since the structure is deformed. The variations are assumed to be slow compare to the control loop dynamic. The cylinder chambers are each fitted with a pressure sensor. Position, velocity and acceleration are provided by sensors on the piston rod.

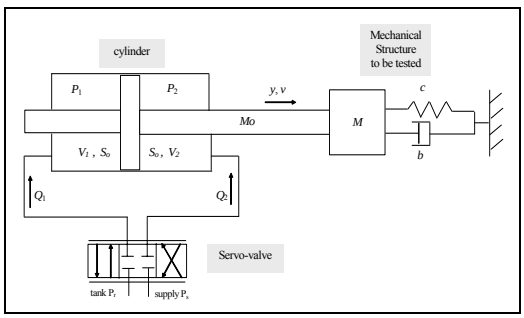

Figure 4. *Electrohydraulic system connected to a mechanical structure to be tested*

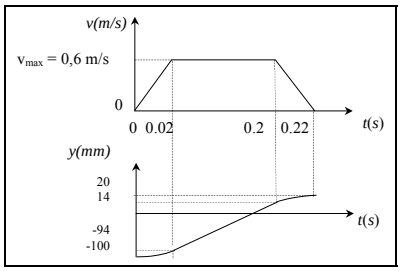

Figure 5. *Piston rod velocity and trajectory*

4.2. *Plant modeling* (Cloy *et al,* 1980)

The complete plant model is obtained from the models of the electrohydraulic servovalve, of the cylinder and of the mechanical part. All the notations are given in the table 1.

Variable Names	Variable definitions	Values
P_s	supply pressure	240 bar
P_r	tank pressure	7.5 bar
P_1, P_2	cylinder chamber pressures	bar
P_{P1}	hydrostatic bearings pressure	236 bar
P_{P2}	hydrostatic bearings pressure	212 bar
B	Bulk modulus	10^9 bar
Q_1, Q_2	mass flow to the cylinder chambers from the servo-valve	m^3/s
V_1 , V_2	cylinder chamber volumes	m^3
V_0	cylinder half-volume	245.10^{-7} m^3
M_0	cylinder rod mass	31.8 Kg
S_0	cylinder rod effective area	243.10^{-6} m²
M	mechanical structure mass	0, 40 or 80 Kg
c	mechanical structure spring	2000, 6000 or12000 N/m
B	mechanical structure viscous coefficient	86 N/m.s
y	cylinder rod position	m
v	cylinder rod velocity	m/s
k_a	Amplification stage gain	0.38 m/A
ω_a	Cut-off frequency of the amplification stage of the servovalve	942 rad/s
k_3	Mass flow gain	$4.5*10^{-5}$ $(m^3/s)/m$
λ	Cylinder leakage coefficient	1.10^{-11} s^{-1}
λ_p	hydrostatic bearings leakage coefficient	$0{,}5.10^{-12}$ s^{-1}

Table 1. *Notations*

The electrohydraulic servovalve is composed of several stages whose main ones are the amplification stage and the flow stage. In the amplification stage, a spool is actuated by an electromechanical system with the input current u as control effort. This stage is modeled by the following transfer function:

$$\frac{Y_i(s)}{U(s)} = \frac{k_a}{\frac{s}{\omega_a} + 1}, \qquad [8]$$

with y_i the spool position, u the current input.

In the flow stage, the spool slides in a sleeve which controls the flows provided to the cylinder chambers. To model these flows, the Bernoulli equation is applied between two points of the sleeve.

The mass flow rate Q is thus proportional to $S\sqrt{\Delta P}$, where S is the effective area of the restrictions of the sleeve and ΔP the pressure-difference between the two points. Given that S is proportional to y_i and that leaks can be neglected, the flow mass rates to each cylinder chamber, Q_1 and Q_2, are described by:

$$\begin{aligned} Q_1(y_i, P_1) &= \begin{cases} k_3 y_i \sqrt{|P_s - P_1|}\, sign(P_s - P_1) & \text{for } y_i \geq 0 \\ k_3 y_i \sqrt{|P_1 - P_r|}\, sign(P_1 - P_r) & \text{for } y_i < 0 \end{cases} \\ Q_2(y_i, P_2) &= \begin{cases} -k_3 y_i \sqrt{|P_2 - P_r|}\, sign(P_2 - P_r) & \text{for } y_i \geq 0 \\ -k_3 y_i \sqrt{|P_s - P_2|}\, sign(P_s - P_2) & \text{for } y_i < 0 \end{cases}. \end{aligned} \qquad [9]$$

Moreover, the leakage are considered as laminar (with coefficient λ) between the two chambers and laminar (with coefficient λ_p) between each chamber and the hydrostatic bearings characterised by the pressures P_{P1} and P_{P2}. So, the leakage mass flow rates are written:

$$\begin{aligned} Q_{1\text{leakage}} &= \lambda(P_1 - P_2) + \lambda_p(P_1 - P_{P1}) \\ Q_{2\text{leakage}} &= \lambda(P_1 - P_2) + \lambda_p(P_{P2} - P_2) \end{aligned} \qquad [10]$$

The cylinder is modeled using the thermodynamic equation giving the pressure behaviour: $\frac{V}{B}\frac{dP}{dt} + \frac{dV}{dt} = Q$, where B is the bulk isotherm modulus, and where V, P and Q are respectively: volume, pressure and mass flow rate in a cylinder chamber. For the electrohydraulic system under study, the mass flow rates are deduced from the mass flow rates to each chamber Q_1 and Q_2 given by relation [9] and the leakage mass flow rates given by relation [10]. Volumes are: $V_1 = V_0 + S_0 y$ and $V_2 = V_0 - S_0 y$, where S_0 is the cylinder rod effective area and V_0 the half-volume. Thus the pressure behaviors in the two cylinder chambers are described by:

$$\frac{\mathrm{d}P_1}{\mathrm{d}t} = \frac{B}{V_0 + S_0 y}\left(Q_1 - Q_{1\text{leakage}} - S_0 v\right) \text{ and } \frac{\mathrm{d}P_2}{\mathrm{d}t} = \frac{B}{V_0 - S_0 y}\left(Q_2 - Q_{2\text{leakage}} + S_0 v\right) \qquad [11]$$

Concerning the mechanical part, the model is obtained from the fundamental dynamic equation:

$$\left(M + M_0\right)\frac{\mathrm{d}^2 y}{\mathrm{d}t^2} = S_0 P_1 - S_0 P_2 - bv - cy - F_\mathrm{f}\,, \qquad [12]$$

where F_f represents the Coulomb friction force (F_c), the static friction force (F_s) and the Stribeck friction force (with the coefficient v_s) (Olsson *et al*, 1998) and expresses:

$$F_\mathrm{f} = F_\mathrm{c}\mathrm{sign}(v) + (F_\mathrm{s} - F_\mathrm{c})e^{\left(-\frac{v}{v_\mathrm{s}}\right)^2}\mathrm{sign}(v)\,. \qquad [13]$$

Finally, as the controlled output is the velocity v, the state-space model of the electrohydraulic system obtained from equations [1], [9] , [11] and [13] is:

$$\begin{cases} \dot{\mathbf{X}} = \mathbf{f}_1(\mathbf{X}) + \mathbf{g}(\mathbf{X})u \quad \text{for } y_\mathrm{i} \geq 0 \\ \dot{\mathbf{X}} = \mathbf{f_2}(\mathbf{X}) + \mathbf{g}(\mathbf{X})u \quad \text{for } y_\mathrm{i} < 0 \qquad \text{with } \mathbf{X} = \begin{pmatrix} P_1 & P_2 & v & y & y_\mathrm{i} \end{pmatrix}^\mathrm{T}. \\ \mathbf{Y} = \mathbf{h}(\mathbf{X}) \end{cases} \qquad [14]$$

This is a five-order nonlinear model where $\mathbf{f}_1$, $\mathbf{f}_2$, $\mathbf{g}$ and $\mathbf{h}$ are defined by:

$$\mathbf{f}_1(\mathbf{X}) = \begin{pmatrix} \frac{B}{V_0 + S_0 y}\left(-S_0 v + k_\mathrm{i} y_\mathrm{i}\sqrt{|P_\mathrm{s} - P_1|}\,sign(P_\mathrm{s} - P_1) - \lambda(P_1 - P_2) - \lambda_\mathrm{p}\left(P_1 - P_{\mathrm{P}1}\right)\right) \\ \frac{B}{V_0 - S_0 y}\left(S_0 v - k_\mathrm{i} y_\mathrm{i}\sqrt{|P_2 - P_\mathrm{r}|}\,sign(P_2 - P_\mathrm{r}) - \lambda(P_1 - P_2) - \lambda_\mathrm{p}\left(P_2 - P_{\mathrm{P}2}\right)\right) \\ \frac{1}{M + M_0}\left(SP_1 - SP_2 - K_\mathrm{r}(y - y_0) - bv - F_\mathrm{frot}\right) \\ v \\ -\omega_\mathrm{a} y_\mathrm{i} \end{pmatrix}, \qquad [15]$$

$$\mathbf{f}_2(\mathbf{X}) = \begin{pmatrix} \frac{B}{V_0 + S_0 y}\left(-S_0 v + k_\mathrm{i} y_\mathrm{i}\sqrt{|P_1 - P_r|}\,sign(P_1 - P_r) - \lambda(P_1 - P_2) - \lambda_\mathrm{p}\left(P_1 - P_{\mathrm{P}1}\right)\right) \\ \frac{B}{V_0 - S_0 y}\left(S_0 v - k_\mathrm{i} y_\mathrm{i}\sqrt{|P_\mathrm{s} - P_2|}\,sign(P_\mathrm{s} - P_2) - \lambda(P_1 - P_2) - \lambda_\mathrm{p}\left(P_2 - P_{\mathrm{P}2}\right)\right) \\ \frac{1}{M + M_0}\left(SP_1 - SP_2 - K_\mathrm{r}(y - y_0) - bv - F_\mathrm{frot}\right) \\ v \\ -\omega_\mathrm{a} y_\mathrm{i} \end{pmatrix}, \qquad [16]$$

$$\mathbf{g}(\mathbf{X}) = \begin{pmatrix} 0 \\ 0 \\ 0 \\ 0 \\ \omega_a \end{pmatrix} \qquad [17]$$

and

$$\mathbf{h}(\mathbf{X}) = v\ , \qquad [18]$$

where $k_i = k_a * k_3$.

4.3. *Input-output linearization of the electrohydraulic testing bench*

4.3.1. *Separation into slow and fast subsystems*

The singular perturbation technique is applied in order to get a nonlinear fast subsystem and a linear slow subsystem which contains all the uncertain parameters.

Let consider $\mathbf{X}_f = (P_1 \quad P_2 \quad y_i)^T$ as the fast state-variable vector and $\mathbf{X}_s = (v \quad y)^T$ as the slow state-variable vector. This assumption is justified when computing the velocity of each variable with the help of the relation [3]:

$$v_{y_i} = 942; v_{P_1} = 3.49 * 10^8; v_{P_2} = 1.62 * 10^9 : v_v = 1.19; v_y = 0. \qquad [19]$$

It is then possible to define a fast subsystem:

$$\begin{aligned} \dot{\mathbf{X}}_f &= \mathbf{f}_{f1}(\mathbf{X}_s, \mathbf{X}_f) + \mathbf{g}_f(\mathbf{X}_s, \mathbf{X}_f) u_f \quad \text{if } y_i \geq 0 \\ \dot{\mathbf{X}}_f &= \mathbf{f}_{f2}(\mathbf{X}_s, \mathbf{X}_f) + \mathbf{g}_f(\mathbf{X}_s, \mathbf{X}_f) u_f \quad \text{if } y_i < 0 \end{aligned} \qquad [20]$$

with

$$\mathbf{f}_{f1}(\mathbf{X}_s, \mathbf{X}_f) = \begin{pmatrix} \dfrac{B}{V_0 + S_0 y}\left(-S_0 v + k_i y_i \sqrt{|P_s - P_1|}\, sign(P_s - P_1) - \lambda(P_1 - P_2) - \lambda_p(P_1 - P_{P1}) \right) \\ \dfrac{B}{V_0 - S_0 y}\left(S_0 v - k_i y_i \sqrt{|P_2 - P_r|}\, sign(P_2 - P_r) - \lambda(P_1 - P_2) - \lambda_p(P_1 - P_{P1}) \right) \\ -\omega_a y_i \end{pmatrix} \qquad [21]$$

$$\mathbf{f}_{f2}(\mathbf{X}_s,\mathbf{X}_f)=\begin{pmatrix}\frac{B}{V_0+S_0y}\left(-S_0v+k_iy_i\sqrt{|P_1-P_r|}sign(P_1-P_r)-\lambda(P_1-P_2)-\lambda_p(P_1-P_{P1})\right)\\ \frac{B}{V_0-S_0y}\left(S_0v-k_iy_i\sqrt{|P_s-P_2|}sign(P_s-P_2)-\lambda(P_1-P_2)-\lambda_p(P_1-P_{P1})\right)\\ -\omega_a y_i\end{pmatrix}, \quad [22]$$

$$\mathbf{g}_f(\mathbf{X}_s,\mathbf{X}_f)=\begin{pmatrix}0 & 0 & \omega_a\end{pmatrix}^T \quad [23]$$

and

$$\mathbf{u}_f = u\,. \quad [24]$$

For this subsystem, the output is the pressure-difference P_1-P_2. This output is also the input of the slow subsystem defined by:

$$\dot{\mathbf{X}}_s=\mathbf{f}_s(\mathbf{X}_s,\mathbf{X}_f)+\mathbf{g}_s(\mathbf{X}_s,\mathbf{X}_f)u_s\,, \quad [25]$$

where

$$\mathbf{f}_s(\mathbf{X}_s,\mathbf{X}_f)=\begin{pmatrix}\frac{1}{M+M_o}\left(-cy-bv-F_f\right)\\ v\end{pmatrix}, \quad [26]$$

$$\mathbf{g}_s(\mathbf{X}_s,\mathbf{X}_f)=\begin{pmatrix}\frac{S_o}{M+M_o}\\ 0\end{pmatrix}. \quad [27]$$

and

$$\mathbf{u}_s = P_1 - P_2\,. \quad [28]$$

4.3.2. *Description of the system to be linearized*

The input-output linearization is achieved for the fast subsystem whose output $\boldsymbol{Y}_f$ is the pressure-difference. In order to simplify the linearization, only the nonlinear behavior of the system is taken into account. The amplification stage dynamics is thus neglected and the input used is u^*. So, the system to be linearized is defined by:

$$\begin{cases}\dot{\mathbf{X}}_{fl}=\mathbf{f}_{f_l}(\mathbf{X}_s,\mathbf{X}_{f1})+\mathbf{g}_{f1_1}(\mathbf{X}_s,\mathbf{X}_{f1})u^* & \text{if } y_i\geq 0\\ \dot{\mathbf{X}}_{fl}=\mathbf{f}_{f1}(\mathbf{X}_s,\mathbf{X}_{f1})+\mathbf{g}_{f1_2}(\mathbf{X}_s,\mathbf{X}_{f1})u^* & \text{if } y_i<0\\ \mathbf{Y}_f=\mathbf{h}(\mathbf{X})\end{cases} \quad [29]$$

with

$$\mathbf{X}_{\mathrm{f}_1} = \begin{pmatrix} P_1 & P_2 \end{pmatrix}^T , \qquad [30]$$

$$\mathbf{f}_{\mathrm{f}1}(\mathbf{X}_\mathrm{s}, \mathbf{X}_{\mathrm{f}_1}) = \begin{pmatrix} \dfrac{B}{V_0 + S_0 y}\left(-S_0 v - \lambda\left(P_1 - P_2\right) - \lambda_\mathrm{p}\left(P_1 - P_{\mathrm{P}1}\right)\right) \\ \dfrac{B}{V_0 - S_0 y}\left(S_0 v - \lambda\left(P_1 - P_2\right) - \lambda_\mathrm{p}\left(P_1 - P_{\mathrm{P}1}\right)\right) \end{pmatrix}, \qquad [31]$$

$$\mathbf{g}_{\mathrm{f}_{1_1}}(\mathbf{X}_\mathrm{s}, \mathbf{X}_{\mathrm{f}1}) = \begin{pmatrix} \dfrac{B}{V_0 + S_0 y} k_i \sqrt{\left|P_\mathrm{s} - P_1\right|}\, sign(P_\mathrm{s} - P_1) \\ \dfrac{-B}{V_0 - S_0 y} k_i \sqrt{\left|P_2 - P_r\right|}\, sign(P_2 - P_r) \end{pmatrix}, \qquad [32]$$

$$\mathbf{g}_{\mathrm{f}_{1_2}}(\mathbf{X}_\mathrm{s}, \mathbf{X}_{\mathrm{f}1}) = \begin{pmatrix} \dfrac{B}{V_0 + S_0 y} k_i \sqrt{\left|P_1 - P_r\right|}\, sign(P_1 - P_r) \\ \dfrac{-B}{V_0 - S_0 y} k_i \sqrt{\left|P_\mathrm{s} - P_2\right|}\, sign(P_\mathrm{s} - P_2) \end{pmatrix} \qquad [33]$$

$$\mathbf{h}(\mathbf{X}) = P_2 - P_1 . \qquad [34]$$

and u^* defined in the figure 5.

At this stage, the amplification stage dynamics has not been taken into account although it is not negligible. The final control input u is computed by using a band-limited inverse model of the amplification stage behavior. This leads to the scheme of the linearization of the figure 6.

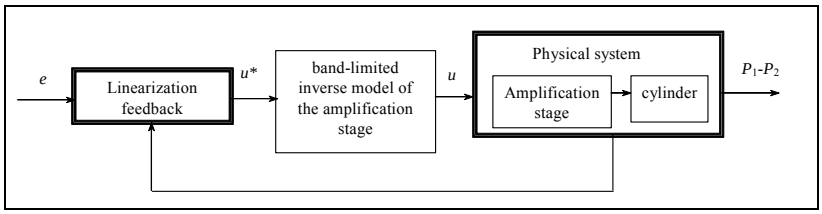

Figure 6. *Scheme of the linearization strategy*

4.3.3. *Input-output linearization under diffeomorphism and static feedback*

The input-output linearization (Isidori, 1989) (Krstic *et al*, 1995) (Fossard *et al*, 1997) (Slotine *et al*, 2001) uses the Lie derivatives. The Lie derivative, $\mathbf{L}_{\mathbf{f}_{\mathrm{fl}}}$, along $\mathbf{f}_{\mathrm{fl}}$ is given by:

$$\mathbf{L}_{\mathbf{f}_{\mathrm{fl}}}(\mathbf{X}_{\mathrm{s}},\mathbf{X}_{\mathrm{fl}}) = \sum_{i=1}^{n} \mathbf{f}_{\mathrm{fl}_i}(\mathbf{X}_{\mathrm{s}},\mathbf{X}_{\mathrm{fl}}) \frac{\partial}{\partial \mathbf{X}_{\mathrm{fl}_i}} . \qquad [35]$$

ρ the relative degree associated with the output is defined by:

$$\rho = \left\{ \inf(l) \in N \ / \ \mathbf{L}_{\mathbf{g}_{\mathrm{fl}_1}} \mathbf{L}_{\mathbf{f}_{\mathrm{fl}}}^{\rho-1} \mathbf{h} \neq 0 \ \text{ if } \ y_i \geq 0, \ \mathbf{L}_{\mathbf{g}_{\mathrm{fl}_2}} \mathbf{L}_{\mathbf{f}_{\mathrm{fl}}}^{\rho-1} \mathbf{h} \neq 0 \ \text{ if } \ y_i < 0 \right\}. \qquad [36]$$

Here, computation leads to $\rho = 1$.

Considering the system described by the relation [29], the decoupling term $\Delta(\boldsymbol{X}_{\mathrm{s}},\boldsymbol{X}_{\mathrm{fl}})$ used in the input-output linearization is thus given by:

$$\Delta(\mathbf{X}_{\mathrm{s}},\mathbf{X}_{\mathrm{fl}}) = \mathbf{L}_{\mathbf{g}_{\mathrm{fl}_1}} \mathbf{h}(\mathbf{X}_{\mathrm{s}},\mathbf{X}_{\mathrm{fl}}) = Bk_{\mathrm{i}} \left[\frac{\sqrt{P_s - P_1}}{(V_{\mathrm{o}} + Sy)} + \frac{\sqrt{P_2 - P_r}}{(V_{\mathrm{o}} - Sy)} \right] \ \text{if } y_{\mathrm{i}} \geq 0, \qquad [37]$$

$$\Delta(\mathbf{X}_{\mathrm{s}},\mathbf{X}_{\mathrm{fl}}) = \mathbf{L}_{\mathbf{g}_{\mathrm{fl}_2}} \mathbf{h}(\mathbf{X}_{\mathrm{s}},\mathbf{X}_{\mathrm{fl}}) = Bk_{\mathrm{i}} \left[\frac{\sqrt{P_1 - P_r}}{(V_{\mathrm{o}} + Sy)} + \frac{\sqrt{P_s - P_2}}{(V_{\mathrm{o}} - Sy)} \right] \ \text{if } y_{\mathrm{i}} < 0 \qquad [38]$$

and the compensation term $\Delta_{\mathrm{o}}(\boldsymbol{X}_{\mathrm{s}},\boldsymbol{X}_{\mathrm{fl}})$ is given by:

$$\Delta_{\mathrm{o}}(\mathbf{X}_{\mathrm{s}},\mathbf{X}_{\mathrm{fl}}) = \mathbf{L}_{\mathbf{f}_{\mathrm{fl}}} \mathbf{h}(\mathbf{X}_{\mathrm{s}},\mathbf{X}_{\mathrm{fl}}) = \frac{-B[Sv + \lambda(P_1 - P_2)]}{\frac{1}{V_o + Sy} + \frac{1}{V_o - Sy}} - \frac{B\lambda_p(P_1 - P_{p1})}{V_o + Sy} + \frac{B\lambda_p(P_2 - P_{p2})}{V_o + Sy} . \qquad [39]$$

Then the state feedback defined by

$$u^*(\mathbf{X}_{\mathrm{s}},\mathbf{X}_{\mathrm{fl}}) = \frac{1}{\Delta(\mathbf{X}_{\mathrm{s}},\mathbf{X}_{\mathrm{fl}})} \left[ke - \alpha Y_l - \Delta_{\mathrm{o}}(\mathbf{X}_{\mathrm{s}},\mathbf{X}_{\mathrm{fl}}) \right], \qquad [40]$$

$k = 7.10^8$ and $\alpha = 2.10^3$, transforms the nonlinear system into the linearized system:

$$H(s) = \frac{k}{s + \alpha_0} . \qquad [41]$$

Usually, the input-output linearized behavior is defined by the transfer function of a ρ-order integrator. Here, the state feedback is more than a simple input-output linearizing feedback since it also contains a part of the tracking feedback. Parameter

α is also used to avoid that the nominal ρ-order integrator system becomes a system with right half-plane poles if the actual nonlinear plant is perturbed. Parameters α and *k* are computed so that the frequency response of *H(s)* is comparable to the first-order linear model of the nominal nonlinear plant.

Finally, to achieve the description of the input-output linearization, the next equation gives the band-limited inverse model of the amplification stage:

$$\frac{U(s)}{U^*(s)} = \frac{\frac{s}{5000}+1}{\frac{s}{\omega_a}+1}. \qquad [42]$$

Whereas the linearization is all the better than the inverse model is not too quickly band-limited, the inverse model must not be band-limited in too high frequency for the input signal *u* not to be too sensitive to noise.

4.3.4. *Advantages of the proposed input-output linearization*

The first advantage of designing the linearization on the fast subsystem without taking into account the amplification stage dynamic and the mechanical load is that the relative degree is smaller than the one obtained with the linearization on the global system (ρ equals to 1 instead of 4). So the input-output feedback is simpler and easier to implement. The other advantage is that this feedback does not depend on the main uncertain parameters (*M*, *c* and *b*). The input-output linearization of the nonlinear part of the system is almost perfect and thus the behavior of the new system to be controlled is independent of the operating points.

5. Control of the testing bench

5.1. *Scheme of the control system*

The scheme of the control system (Fig.7) includes two feedback loops:

– ① is a feedback for the input-output linearization. The aim of this linearization is to cancel the nonlinear behavior of the actuator.

– ② is a velocity feedback since velocity is the output to be controlled. This robust loop must be designed while taking into account the parametric variations of the mechanical structure.

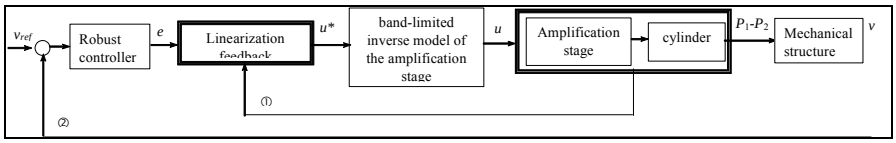

Figure 7. *Scheme of the control system*

5.2. *Control design*

As the control system will be digital, and as Crone design, used for the robust outer-loop, is a continuous frequency-domain approach, the digital control-design problem is transformed into a pseudo-continuous problem using the *z* and *w* transforms. The bilinear *w*-transform is defined by:

$$z^{-1} = \frac{1-w}{1+w} \quad \text{with } w=\mathrm{j}v \text{ and } v = \tan\left(\frac{\omega T_s}{2}\right), \qquad [43]$$

and permits the easy calculation of the frequency response of a *z*-domain transfer function as:

$$F(\mathrm{j}v) = F(z) \text{ with } z = e^{\mathrm{j}\omega T_s} \qquad [44]$$

Here the sampling period is $T_s = 0.2$ ms.

The Crone open-loop transfer function to be optimized is:

$$\beta_0(w) = K\left(\frac{v_{-N^-}}{w}+1\right)^{n_l} \frac{f(w)}{\left(1+w/v_{N^++1}\right)^{n_h}} \prod_{-N^-}^{N^+}\left(\frac{1+w/v_{k+1}}{1+w/v_k}\right)^{a_k} \left(\Re_{/i}\left[\left(C_k\frac{1+w/v_{k+1}}{1+w/v_k}\right)^{\mathrm{i}b_k}\right]\right)^{-\mathrm{sign}(b_k)}, \qquad [45]$$

where *f(w)* is a function that takes into account the two plant right half-plane zeros closed to $v = +1$ which appeared when the bilinear *w*-transformation has been applied.

Here, optimization uses $N^+ = N^- = 1$, so a set of three band-limited generalized templates is used. The behavior of the open-loop transfer function at low and high frequencies is fixed with: $n_l = 0$ and $n_h = 4$. The required resonant peak M_r chosen for the nominal plant is 1dB and the constraints on the sensitivity functions are defined from:

– the maximum plant input (100mA),

– the Fourier transform of the required trajectory.

The constraints on the sensitivity functions are thus given by:

– the maximum magnitude T_{max} of the complementary sensitivity function set at 1 dB,

– the maximum magnitude S_{max} of the sensitivity function set at 6dB.

– the maximum magnitude CS_{max} of the input sensitivity function set at 5dB.

Fig.8 shows the optimal open-loop Nichols loci. The optimal parameters position the frequency uncertainty domains to minimize the variation of the M resonant peak. Then maximal value of sensitivity functions are T_{max} = 0.93 dB and S_{max} = 4.35 dB. The optimal resonant pseudo-frequency is 0.03 (equivalent of ω = 300 rad/s) and optimal parameters are as following:

$$v_{-1} = 0.0005 ; v_0 = 0.001 ; v_1 = 0.3 ; v_2 = 0.7 ; a_{-1} = 1 ; b_{-1} = 0 ; b_0 = 0.38 ; a_1 = 0.5 ; b_1 = 0 .$$

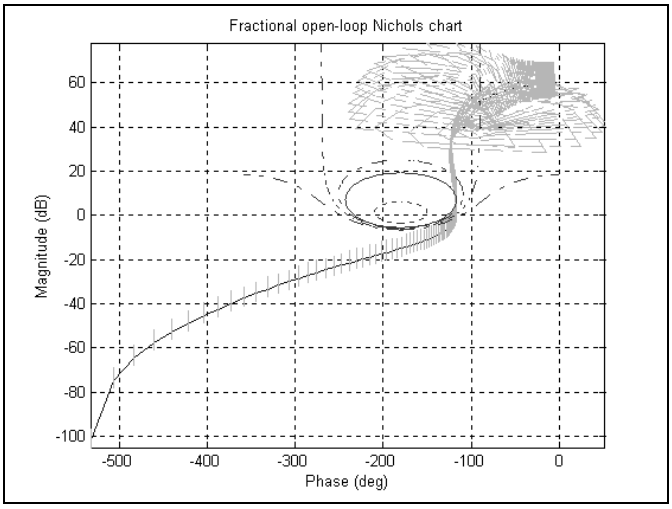

Figure 8. *Optimal open-loop Nichols and uncertainty domains*

The synthesized pseudo-continuous rational controller obtained for the velocity feedback is a seven-order filter:

$$C(v) = 5.10^{-3} \frac{\left(\frac{v^2}{0{,}00095^2} + \frac{2*0{,}06}{0{,}00095}v + 1\right)\left(\frac{v}{0{,}011} + 1\right)\left(\frac{v}{0{,}271} + 1\right)\left(\frac{v}{0{,}373} + 1\right)}{v\left(\frac{v}{0{,}00033} + 1\right)\left(\frac{v}{0{,}002} + 1\right)\left(\frac{v^2}{0{,}581^2} + \frac{2*0{,}6}{0{,}581}v + 1\right)\left(\frac{v}{1{,}756} + 1\right)^2} . \quad [46]$$

The digital controllers $C(z^{-1})$ is obtained from $C(v)$ using the inverse w-transform defined above.

5.3. *Simulation results*

So that the simulation is nearer to reality as possible, the nonlinear friction force of the hydraulic cylinder is modeled by a 700N static friction, a 500N Coulomb friction and a Stribeck parameter v_s equal to 0.5m/s. Moreover, by refering to some sensors data-sheets, noises have been added on measures:

– for the acceleration, noise is 0.24mg and thermal zero offset is 2 mg/°C;

– for the pressure transducers, noise is 60000 Pa and thermal zero offset is 12000 Pa/°C;

– for the displacement transducer, thermal zero offset is 0.075mm/°C.

– for the velocity transducer, noise is 0.1 mm/s and thermal zero offset is 0.55 mm/s/°C.

Fig.8 presents the simulated output v with the Crone controller for the nominal and extremal parametric states of the mechanical structure. This result is compared with that obtained with a PID controller computed to have the same gain cross-over frequency and the same lowest overshoot than the CRONE controller. The PID controller is defined by:

$$C_{\mathrm{PID}}(v) = Co\left(\frac{v_{\mathrm{i}}}{v}+1\right)\frac{\dfrac{v}{v_1}+1}{\dfrac{v}{v_2}+1}\,\frac{1}{\dfrac{v}{vf}+1} \qquad [47]$$

with v_i =0.003, v_f = 0.3, v_1 =0.0252, v_2 = 0.0357 and with Co computed to have a gain of 0 dB at the gain cross-over frequency, so Co = 0.128.

As the Crone approach permits to manage phase-margin and also other stability margins as gain-margin, magnitude peaks,...for plants with right half-plane zeros while taking into account the plant perturbations, the Crone controller gives better results since the overshoot varies less than with the PID (Fig.9): the overshoot varies from 4% to 9% with the Crone controller and from 4% to 15% with the PID controller.

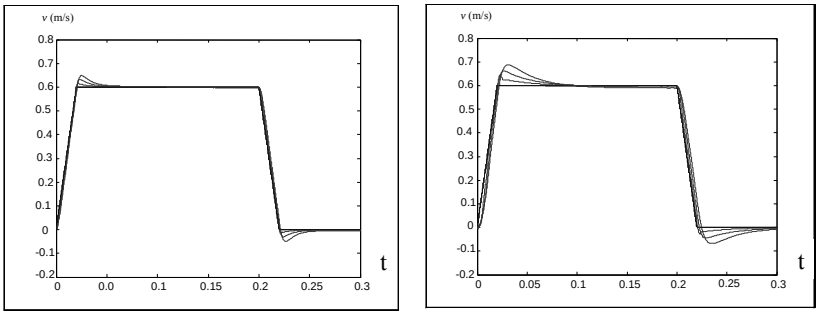

(a) (b)

Figure 9. *Simulated controlled output for three states of the mechanical structure with the Crone controller (a) and with a PID controller (b)*

As it is well known that the derivative action of the PID controller may lead to robustness problem, another PID is designed only using its integral and low-pass parts ($v_1 = v_2$ and Co = 0.107). In this case, the overshoot varies from 9% to 15% (Fig. 10). The variation is lower but it seems that it is not possible to guaranty a low overshoot (it seems that the maximal overshoot can not be less than 15%).

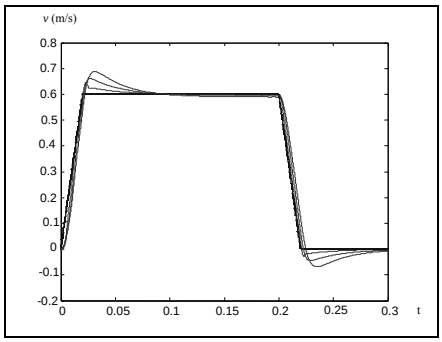

Figure 10. *Simulated controlled output for three states of the mechanical structure with a PID controller without derivative action*

In the case of maximal values of the mechanical structure parameters, Fig.11 shows that the plant input *u* is less than 100 mA. Thus, the plant is not too much

solicited. For other loads, plant inputs are similar. One can also notice that the noise on this input is a consequence of the noises added on the measures.

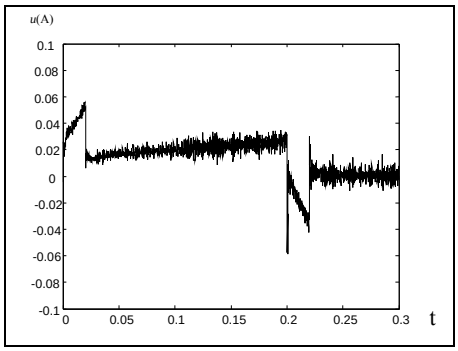

Figure 11. *Plant input with the CRONE controller for the maximal values of the mechanical structure parameters.*

A further simulation is achieved to verify the behaviour of the control system faced with a quick variation of the stiffness parameter. The initial value of the stiffness is 12000N/m and its final value is 2000N/m. Fig.12 shows that the perturbation is better rejected with the CRONE controller than with the PID controller.

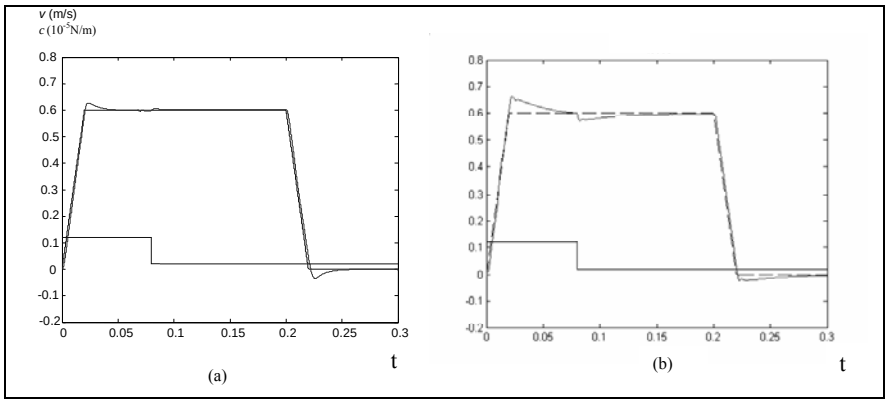

Figure 12. *Simulated controlled velocity (--) with a quick variation of the stiffness parameter (—) for the CRONE controller (a) and the PID controller (b)*

6. Conclusion

Singular perturbation technique can be used successfully in the control strategy of a hydraulic testing bench whose some parameters are uncertain. It allows to simplify the plant control linearization and the remaining linearities are considered as perturbations. Crone control-system design (based on fractional differentiation) is finally implemented to reject perturbations and to obtain good performances despite the uncertainties. Final results demonstrate the efficiency of the proposed control-system design method.

In a more general context, the method proposed in this article can be applied to any nonlinear and uncertain system with two time-scales dynamics.

7. Bibliography

Banavar R., Aggarwal V., "A loop transfer recovery approach to the control of an electro-hydraulic actuator ", *Control Engineering Practice*, Vol.6, p.837-845, 1998.

Cloy M.C., Martin H.K., "*Control of fluid power, Analysis and Design*", John Wiley and Sons, New York, 1980.

Fossard A.J., Normand-Cyrot D., "*Nonlinear Systems-Control*", Vol.3, Chapman&Hall and Masson, 1997.

Isidori A., "*Nonlinear control systems*", Springer Verlag, 2nd edition, 1989.

Krstic M., Kanellakopoulos I.,Kokotovic P. V., "*Nonlinear and Adaptive Control Design*", Wiley, New York, 1995.

Landau I.D., Rey D., Karimi A., Voda A.,Franco A., "*A Flexible Transmission System as a Benchmark for Robust Digital Control*", European Journal of Control, Vol.1, n°2, 1995.

Lanusse P., Pommier V., Oustaloup A., "*Fractional control-system design for a hydraulic actuator*", 1st IFAC Conference on Mechatronics Systems, 18-20 Septembre, Darmstadt, Germany, 2000.

Miller K.S., Ross B., "*An introduction to the fractional calculus and fractional differential equations*", John Wiley & Sons Inc., New York, 1993.

Olsson H., Aström K.J., Canudas de Wit C., Gäfvert M., Lischinsky P., "*Friction Models and Friction Compensation*", European Journal of Control, Vol.4, n°3, 1998.

Oustaloup A., "*La dérivation non entière : théorie, synthèse et applications*", Editions HERMES, Paris, 1995.

Oustaloup A., Lanusse P., Mathieu B., "*Robust control of SISO plants: the CRONE control*", ECC'95, Rome, Italy, 1995.

Oustaloup A., Mathieu B., Lanusse P., "*The CRONE control of resonant plants: application to a flexible transmission*", European Journal of Control, Vol. 1, pp. 113-121, 1995.

Oustaloup A., Mathieu B., "*La commande CRONE : du scalaire au multivariable*", Editions HERMES, Paris, 1999.

Oustaloup A., Sabatier J., Lanusse P., "*From fractal robustness to the CRONE Control*", Fractional Calculus and Applied Analysis: An international Journal for Theory and Applications, Vol. 2, n° 1, 1999.

Oustaloup A., Levron F., Nanot F, Mathieu B., "*Frequency band complex non integer differentiator: Characterization and synthesis*", IEEE Transactions on Circuit and Systems, Vol 47, n° 1, p 25-40, 2000.

Pommier V., Lanusse P., Sabatier J., Oustaloup A., "*Input-output linearization and fractional robust control of a non linear system*", European Control Conference ECC01, 4-7 Septembre, Porto, Portugal, 2001.

Samko S.G., Kilbas A.A., Marichev O.I., "*Fractional integrals and derivatives*", Gordon and Breach Science Publishers, 1993.

Slotine, Li, "*Applied Nonlinear Control*", Prentice-Hall, 1991.